VOID REDUCTION IN OUT-OF-AUTOCLAVE PROCESSING OF CARBON FIBER EPOXY COMPOSITES BY REINFORCING INTERLAMINAR REGIONS USING VERTICALLY ALIGNED CARBON NANOTUBES

Yiying Zhang, Mackenzie Devoe, Ben Bancroft, Heather Conway, Dan Chebot, Ryan D. Williams, Dina Deresh, Jay Maxwell and Christopher Gouldstone

N12 Technologies, Inc., 85 Bolton St., Cambridge, MA 02148, USA
Email: yzhang@n12technologies.com, Web Page: http:// http://www.n12technologies.com

Keywords: out-of-autoclave, void content, carbon nanotube, ILSS, OHC

Abstract
Baseline and vertically aligned carbon nanotube (VACNT)-reinforced quasi-isotropic carbon fiber epoxy laminates were fabricated in parallel using out-of-autoclave (OOA) resin systems. The composite parts were tested for interlaminar shear strength (ILSS) and open hole compression (OHC) strength. High-resolution large-area maps for cross-section views of entire ILSS specimens are obtained by stitching images taken in secondary electron and backscattered electron imaging modes simultaneously to reveal the global void distribution and crack propagation. Image analysis and X-ray micro-CT were employed to assess void content. Results show VACNT-reinforcement greatly reduces void content in OOA parts. Nearly void-free OOA laminates incorporating VACNTs can be produced with less-stringent and shorter processes than otherwise required. ILSS and OHC strength are improved for up to 33% and 7%, respectively, for cross-ply epoxy laminates, through a combination of direct crack-arresting and reduced porosity. This novel design of hierarchical composite structure with interlaminar VACNT reinforcement has been successfully applied to multiple resin systems, and can be implemented within industry-standard composite manufacturing processes and requires no special tools.

1. Introduction

Out-of-autoclave (OOA) or oven vacuum bag (OVB) processing has matured into an excellent alternative to the traditional autoclave composite manufacturing, for its competitive quality and capacity with significantly simpler processing requirements and lower costs. However, void reduction within composites remains a challenge in this process due to the lower compaction pressure compared to autoclave curing [1-3]. In OOA composite fabrication, voids are readily formed as a result of moisture, entrapped air, escaped volatiles or poor vacuum. Higher void content can be detrimental to mechanical properties of composites, particularly interlaminar shear strength (ILSS) [4-5]. Critical porosity values in various resin systems for ILSS performance have been estimated to be less than 1% [4-6]. This low porosity value is also similar to the target for typical aerospace-grade composites, which is low enough to limit the effect of porosity on the mechanical performance [3, 7].

Void formation is governed by many factors including physical and chemical characteristics of prepreg, ply orientation, lay-up method, debulking, laminate size and geometry, bagging and curing (temperature, vacuum, pressure, etc.) as well as humidity [1-2, 8]. Dynamics of void initiation and growth during processing and the resultant shape and size of voids have been investigated [2-3]. For

Excerpt from ISBN 978-3-00-053387-7

certain prepreg systems, to limit void formation permeability needs to be ensured with the optimized pressure [5] and duration of pressure [9], which increases the processing challenge. Additionally, much work has been done to optimize the rheological properties of the polymer matrix to assist in evacuation of voids.

Volatiles or air bubbles migrate mostly along fiber directions during curing and compaction, while diffusion through ply thickness can take an extremely long time, rendering void reduction during OOA processing impractical [3, 10]. Therefore, channels acting as air pathways, such as partial impregnations [2-3] or rough surfaces of prepreg layers [10], have been attempted in recent work, for air permeability/evacuation before consolidation.

In this work, an alternative is achieved by employing vertically aligned carbon nanotubes (VACNTs). Interlaminar VACNTs are shown to provide uniform inter-ply breathing paths before curing, leading to significant void reduction in OOA composite parts. In addition, preliminary results have also demonstrated that using VACNTs for interlaminar reinforcement could toughen the inter-ply structure and prevent delamination [11], resulting in significant improvements in fracture toughness [12], ILSS fatigue life [13], L-shape laminate bending and open hole compression (OHC) strength [14].

Void content in composites can be measured by multiple methods, including acid digestion and density measurement (ASTM standard D3171-11 and ASTM standard D792), microscopy and image analysis [15], ultrasound C-scan [4-5], and X-ray computed tomography (CT) [16-17]. Acid digestion is a destructive method, and tends to have a relatively large standard deviation, causing the test results to be inaccurate especially for low void contents [18]. Ultrasonic attenuation can be affected by the distribution, location, shape, and size of the voids, which can result from the handling and production of the prepreg materials as well as the aforementioned processing parameters [5, 7]. For these reasons, microscopy imaging and micro-CT are utilized to investigate the composite porosity in this work.

Baseline and VACNT-reinforced composite parts were fabricated out-of-autoclave using two prepreg materials and tested for ILSS and OHC strength. VACNTs acting as air pathways during processing are identified using electron microscopy. Scanning electron micrographs obtained for cross section views are stitched into large-area, high-resolution maps for porosity and fracture analysis on macro-scale specimens. X-ray micro-CT is also used to assess the void content in three-dimensional volume. ILSS and OHC strength are significantly improved with the addition of VACNTs in both prepreg systems, which is attributed to void reduction through VACNT-provided venting channels, as well as the anti-delamination effect by VACNTs stitching between plies.

2. Experimental Section

2.1. Materials

2.1.1. Continuous growth of VACNTs

Vertically aligned carbon nanotubes were produced using a chemical vapor deposition process on a metallic ribbon substrate. The substrate is a continuous tape format which generates long strips of VACNT material running hundreds of meters. The continuous format allows for arrangement and transfer of strips of VACNT forest to the prepreg material for either localized or global reinforcement of the composite part. Height, density and other characteristics of the forest can be controlled quite precisely as needed.

2.1.2. Carbon fiber prepreg

Composite parts in this study were fabricated from TenCate TC350-1 toughened epoxy resin reinforced with IM7 unidirectional fiber, and Newport NCT301-1 toughened epoxy resin reinforced with Mitsubishi 34-700 unidirectional fiber, respectively.

Excerpt from ISBN 978-3-00-053387-7

2.2. Fabrication

Part dimensions and layup formulas are provided in Table 1. Plies were cut precisely for repeatable size and orientation. For the ILSS panels, VACNTs populated all interfacial area (global reinforcement), while for the OHC panels, VACNTs only reinforced the area of 30mm x 38mm centered around the hole (local reinforcement). The as-produced VACNT forest with no chemical modification was transferred, maintaining its alignment and orientation, onto cut plies of pregreg, which were then laid up. After transfer, the forest was partially infused into the matrix, leaving the top of the forest emergent. For both ILSS and OHC parts, the baseline and hybrid parts were debulked and cured in parallel (i.e., laid up at same time, debulked side by side, and cured under same vacuum bag in autoclave or out-of-autoclave), following manufacturer recommended bagging schedules and cure profiles, with the only deliberate difference being the inclusion of VACNTs at ply interfaces.

Table 1. Specifications of composite parts.

Type	*Laminate dimension*	*Layup formula*	*# of plies*	*Specimen dimension*
ILSS	30 mm x 80 mm	[0/90/+45/-45]2s	16	4 mm x 12 mm x 2mm
OHC	300 mm x 300 mm	[+45/0/-45/90]3s	24	38 mm x 300 mm x 3mm D_{hole}^{*} = 6.3 mm

*D_{hole} represents the diameter of hole.

2.3. Characterization

Parts were precisely machined to the desired specimen dimensions (Table 1) for mechanical testing and characterizations. Tested composite parts are polished at cross sections using Allied High Tech Metprep 3™ polisher and treated using PE-25 Venus plasma cleaner to improve imaging contrast. Scanning electron microscopy (SEM) was conducted using a FEI Verios 460L field emission scanning electron microscope (landing voltage: 0.5 kV, current: 50 pA). Cross sections of parts were imaged using secondary electron and backscattered electron imaging modes simultaneously. A representative ILSS specimen was selected for each part, and both secondary and backscattered electron images were taken and automatically stitched into two large-area, high-resolution maps using FEI software Maps 2.1, for global fracture and porosity observations. Uncured prepreg materials were imaged using Nikon Eclipse L200N optical microscope and Zeiss EVO 55 environmental scanning electron microscope (acceleration voltage: 5 kV). Untested cured specimens were also examed using Nikon Metrology (X-Tek) HMXST225 MicroCT system and analyzed using VGStudio MAX 2.2.6.

2.4. Mechanical Testing

All baseline and nano-reinforced hybrid parts were tested for each cure batch, for IM7/TC350-1 and 34-700/NCT301-1 systems, respectively. ILSS testing was performed using an ADMET eXpert 2611 system with a 10kN load cell and Wyoming Test Fixtures short beam shear fixture, according to ASTM standard D2344 [19]. OHC testing was performed using an Instron 5985 floor model system with 250 kN capacity and Wyoming test fixtures open hole compression test fixture, according to ASTM standard D6484 [20]. Seven ILSS specimens were cut from each panel and tested. All three specimens cut from each OHC panel were tested for OHC strength.

3. Results and Discussions

3.1. VACNTs acting as air venting channels

To investigate the morphology of carbon nanotube forests during composite fabrication process, samples were prepared to reveal the micro-/nano-structure evolution at several fabrication steps. The as-grown VACNT forests were first transferred to ply surfaces via resin infusion. Figure 1a shows the cross-section view of a nanotube forest transferred onto a prepreg layer, which was fractured along the fiber direction for imaging purposes. It should be noted that only a small portion (usually below 1 μm) along the forest height is fully infiltrated with resin and the rest of the forest remains air permeable

Excerpt from ISBN 978-3-00-053387-7

(Figures 1a_2 and 1a_3). Since layup and debulking processes are typically conducted at room temperature or temperatures where resin has relatively high viscosity, the air permeability in the forest can be preserved before final cure. The cross-section of a debulked composite part was polished for microscopy observations, but due to the tack of uncured resin, the polishing process caused resin build-ups on the surface, resulting in many morphological features covered (Figure 1b_1). Fortunately, at limited interfacial areas where VACNTs are uncovered, the forest is found slightly deformed or buckled and became more compact due to the compression from resin on both sides during debulking, with the middle of the forest remained permeable, acting as air venting channels (Figures 1b_2 to 1b_4). Finally, the part was cured under vacuum with temperature gradually ramping up, the remained air bubbles and volatiles could migrate to and escape though the breathing path provided by interlaminar VACNTs, before resin viscosity dropped significantly and the path was filled up (Figures 1c_1 to 1c_3). Besides, the low viscosity of resin at elevated temperature also allows further compaction of fibers and interfacial engagement with nanotube forests.

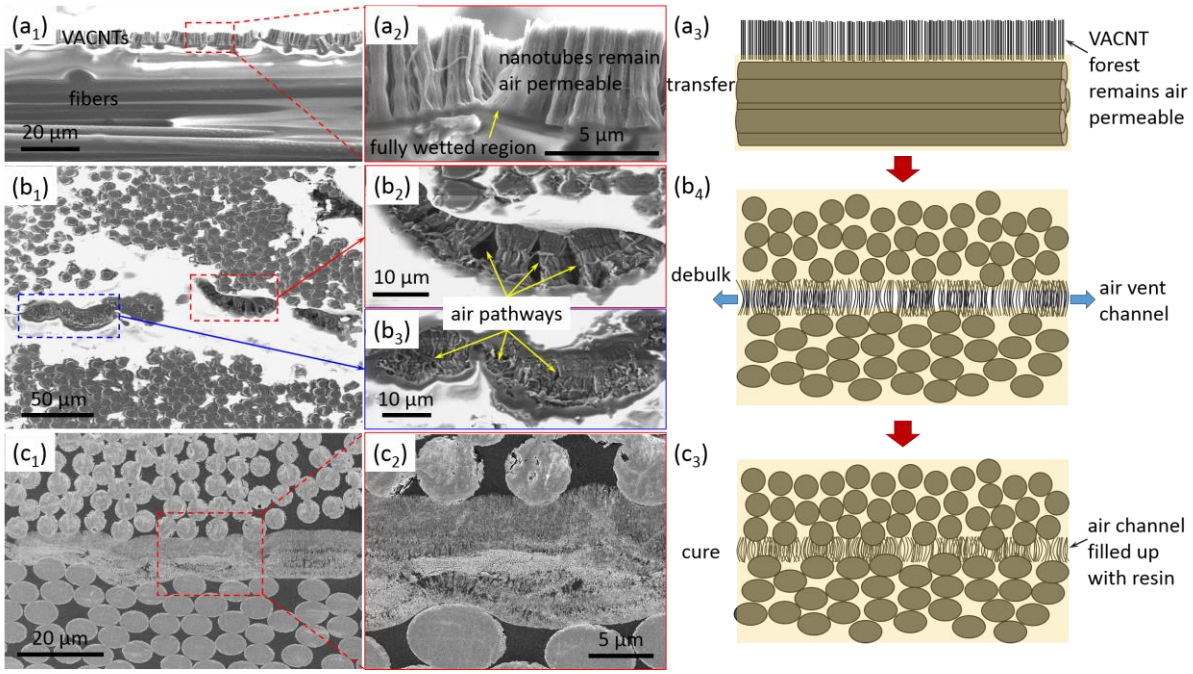

Figure 1. Scanning electron micrographs and corresponding schematics showing interlaminar VACNTs and resin morphology in (a) transferring, (b) debulking and (c) curing processes. Images in a_1, a_2, b_1, b_2, and b_3 are taken by environmental SEM (high brightness of the resin areas are due to the charging effect of uncured resin), and c_1 and c_2 are taken by regular field emission SEM.

3.2. Void content analysis

Figure 2 shows large-area maps obtained by automatic acquisition and stitching of SEM images. Each map covers the entire cross section area (roughly 2mm x 4mm) of an ILSS specimen. Table 2 provides details and properties for eight selected ILSS samples, including four pairs of baseline and nano-enhanced hybrid composites (i.e., A1 and A2, A3 and A4, A5 and A6, A7 and A8, respectively) that are fabricated and cured in parallel. Among them, A1, A2, A5 and A6 are processed with short debulking time and OOA cured; for comparison, A3 and A4 are processed with long debulking time, and A7 and A8 are cured in autoclave. Figures 2a and 2b provide examples of the secondary electron image maps corresponding to the backscattered electron image maps for samples A1 and A2 shown in Figures 2c and 2d, respectively. In this work, backscattered electron images are used for porosity and fracture analysis. However, although the SEM maps have very high resolutions, due to the limits of most image analysis software, a map needs to be compressed into one image below a certain size and consequently loses resolution. In addition, image analysis results are also sensitive to the contrast and brightness settings during image acquisition. As a result, void contents from image analysis tends to be

Excerpt from ISBN 978-3-00-053387-7

much lower than the actual values. Work on optimizing imaging settings and improving image analysis methods for quantitative results are on-going. Therefore, porosity is also investigated by X-ray CT, shown in Table 2, through surface determination within a three-dimensional volume. The CT porosity results agree with the quantitative observations shown in Figure 2.

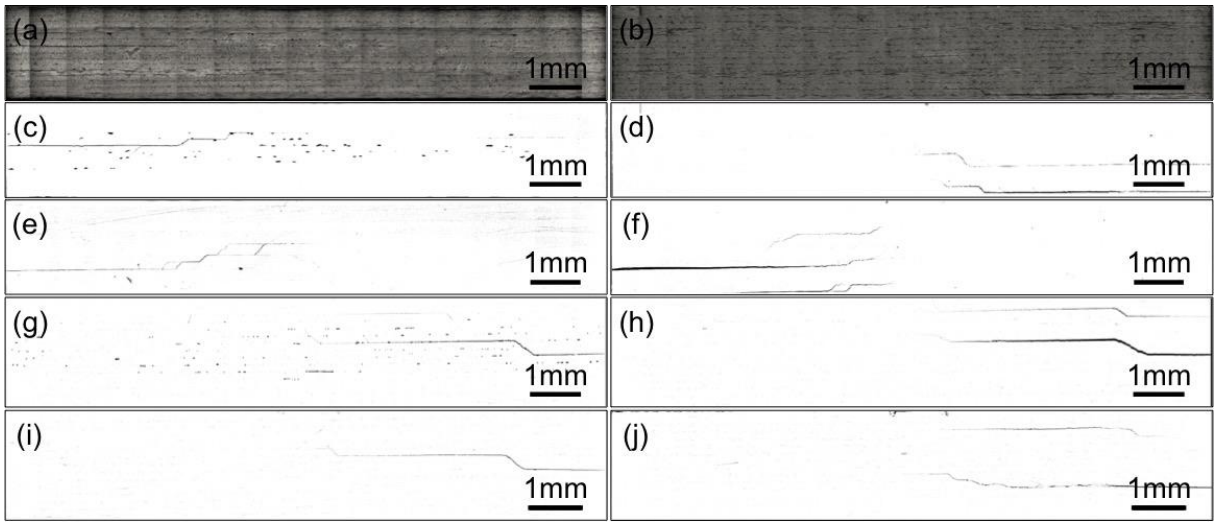

Figure 2. SEM maps generated by automatic acquisition and stitching of individual images. (a) and (b) are obtained in secondary electron imaging mode for samples A1 and A2, respectively. (c) to (j) are obtained in backscattered electron imaging mode for samples A1 to A8, respectively. The left column (a, c, e, g, i) are maps for conventional composite (baseline) specimens; the right column (b, d, f, h, j) are maps for VACNT-reinforced composite (hybrid) specimens.

Table 2. Porosity and interlaminar shear performance of composites fabricated using different prepreg materials and processes.

Sample ID*	type	Fabrication Process	Prepreg Material	Porosity from CT	Average ILSS (MPa)†	COV†‡	Improvement from low BL§
A1	baseline	30-min debulk OOA cure	IM7/ TC350-1	3.55%	87.28	6.38%	-
A2	hybrid			0.91%	111.73	2.20%	28.01%
A3	baseline	8-hr debulk OOA cure		0.94%	108.06	2.00%	23.81%
A4	hybrid			0.83%	116.33	0.85%	33.28%
A5	baseline	1-hr debulk OOA cure	34-700/ NCT301-1	4.01%	82.65	2.34%	-
A6	hybrid			1.00%	89.71	2.32%	8.54%
A7	baseline	1-hr debulk autoclave cure		1.06%	86.26	1.97%	4.37%
A8	hybrid			0.88%	95.15	1.64%	15.12%

**A1 and A2, A3 and A4, A5 and A6, A7 and A8 are fabricated in parallel in one batch, respectively. †Seven specimens were tested under ASTM 2344 guidelines [19] for each sample. ‡COV is coefficient of variation, representing the ratio of the standard deviation to the mean. §Compared to the corresponding OOA baseline sample with short debulking time (A1 or A5) for each prepreg system.*

In samples made using the two prepreg systems (A1 to A4 and A5 to A8), consistent trends are observed: i) compared to the OOA baseline composite with short processing time (A1 or A5), low void content and high ILSS can be achieved by either long time debulking (A3) (Figures 2e, 3a and 3b) or autoclave pressure (A7) (Figure 2i), or using interlaminar VACNTs (A2 or A6) (Figure 2d and 2h) without requiring longer processing or autoclave; ii) by comparing both hybrid parts with low void contents (A2 and A4, A6 and A8), longer processing time or autoclave pressure leads to even better performance, due to the more compact fiber packing and engagement with the carbon nanotube forest (Figures 3c and 3d); iii) by comparing both baseline and hybrid samples with low void contents (A3 and A4, A7 and A8), ILSS is improved with the reinforcement of VACNTs at inter-ply regions, which

Excerpt from ISBN 978-3-00-053387-7

may be attributed to the increased energy barrier (i.e., critical strain energy release rate) for inter-ply fracture. It should be noted that OOA cured hybrid part (A6) is significantly stronger than autoclave cured baseline part (A7), given both having very low void contents, demonstrating the mechanical enhancement from VACNTs. In addition to the improved average strength, in IM7/TC350-1 system, parts with lower void content also have reduced COV values of ILSS results, indicating the more uniform laminate structure. Summarized from Figure 2 and Table 2, with fairly short debulking time (≤1 hr) in OOA processing, the interlaminar VACNT reinforcement reduced void contents to ≤1% (comparable to long debulked or autoclaved parts), and improved ILSS to significantly higher than parts fabricated with long debulking or autoclave curing.

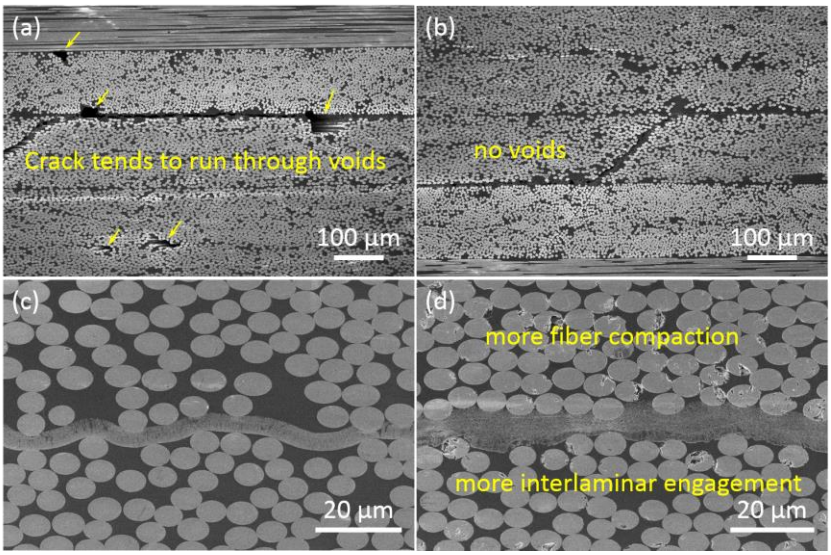

Figure 3. High-resolution SEM images of (a) A1 and (b) A2 samples for global morphology of baseline parts, and (c) A3 and (d) A4 samples for interlaminar morphology of hybrid parts.

In addition to ILSS, OHC strength is also tested for baseline and hybrid samples, named B1, B2, B3 and B4 (B1 and B2, B3 and B4, respectively, are fabricated in parallel), made using the two prepreg materials. The specifications and test results are listed in Table 3. All the parts are processed with extended debulking time to reduce voids in the laminate structure. Yet due to the much larger and thicker dimensions of OHC panels, voids are still observed in some baseline structure even after longer debulking (Figure 4a), but not in hybrid parts (Figure 4b) fabricated in parallel, due to the inclusion of VACNTs. Figures 4c and 4d are close-up views by SEM, revealing the representative micro-/nano-morphology surrounding the cracks. It can be observed that the presence of nanotube forest between plies induces stronger engagement/interaction at the interfaces (Figures 3c, 3d, 4c and 4d), which bonds plies with different orientations. This usually results in intra-ply cracking (Figure 4c) or scission along the forest (Figure 4d) when fractured. In either way, it requires more energy for cracks to grow and consequently leads to a higher load/strength upon fracture. Therefore, the improvement of strength from baseline parts (Table 3) are considered from VACNT contributions on both void reduction and anti-delamination.

4. Conclusions

Baseline and VACNT-reinforced OOA composite parts were fabricated using two prepreg materials, and tested for ILSS and OHC strength. Micro-morphology at interlaminar regions and global void distributions were investigated using optical and electron microscopy as well as the X-ray CT technique. Results indicate that interlaminar reinforcement of VACNTs provides channels for air permeability before consolidation, and requires much shorter processing time to achieve parts with <1% void content. Morphology observations also suggest that the inclusion of interlaminar layer of

Excerpt from ISBN 978-3-00-053387-7

VACNTs enables stronger interactions between plies with different orientations, which increases the critical strain energy release rate for fracture. As a result of void reduction and fracture arrestment by VACNTs, ILSS and OHC strength of the OOA composites are improved for up to 33% and 7%, respectively. In addition to IM7/TC350-1 and 34-700/NCT301-1, this technique has also been successfully applied with significant mechanical improvements in several other prepreg systems, including AS4/8552, T24-4.8/240-E100, C30/E201, etc. (not included in this work).

Table 3. Open hole compression performance of composites fabricated using different prepreg materials and processes.

Sample ID*	type	Fabrication Process	Prepreg Material	Average strength (MPa)†	COV†‡	Improvement from BL§
B1	baseline	10-hr debulk OOA cure	IM7/ TC350-1	312.10	0.31%	-
B2	hybrid			332.74	2.41%	6.61%
B3	baseline	8-hr debulk OOA cure	34-700/ NCT301-1	267.35	0.75%	-
B4	hybrid			281.36	1.86%	5.24%

**B1 and B2, B3 and B4 are fabricated in parallel in one batch, respectively. †Three specimens were tested under ASTM 6484 guidelines [20] for each sample. ‡COV is coefficient of variation, representing the ratio of the standard deviation to the mean. §Compared to the baseline sample (B1 or B3) fabricated in the same batch for each prepreg system.*

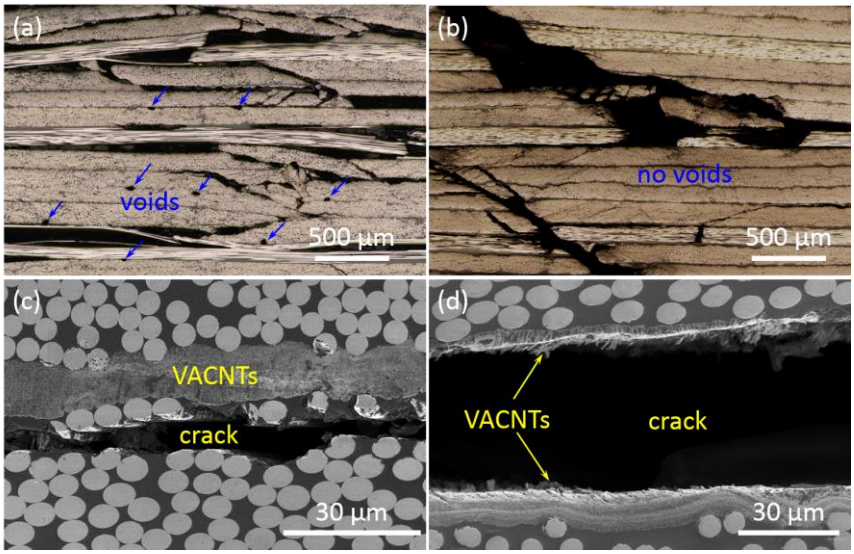

Figure 4. Optical microscopy images of global void distribution in (a) B1 and (b) B2 samples. SEM images of representative interlaminar morphology at fractured regions in (c) B2 and (d) B4 samples.

Acknowledgments

The authors would like to acknowledge TenCate Advanced Composites and Mitsubishi Rayon Group for providing prepreg materials, IM7/TC350-1 and 34-700/NCT301-1, respectively. Environmental SEM and X-ray micro-CT were performed at the Center for Nanoscale Systems (CNS), a member of the National Nanotechnology Infrastructure Network (NNIN), which is supported by the National Science Foundation under NSF award no. ECS-0335765. CNS is part of Harvard University.

References

[1] J. Kay, L. Fahrang, K. Hsiao, G. Fernlund. Effect of process conditions on porosity in out-of-autoclave prepreg laminates. *Proceedings of the 18th International Conference on Composite Materials, Jeju Island, S. Korea,* August 21-26 2011.

Excerpt from ISBN 978-3-00-053387-7

[2] L. Farhang, G. Fernlund. Void evolution and gas transportation cure in out-of-autoclave prepreg laminates. *SAMPE, Long Beach, CA, USA,* May 23-26 2011.
[3] T.A. Cender, J.J. Gangloff Jr., P. Simacek, S.G. Advani. Void reduction during out-of-autoclave thermoset prepreg composite processing. *SAMPE Conference Proceedings, Seattle, WA, USA,* June 2-5 2014.
[4] P.A. Olivier, B. Mascaro, P. Margueres, F. Collombet. CFRP with voids: ultrasonic characterization of localized porosity, acceptance criteria and mechanical characteristics. *Proceedings of 16th International Conference on Composite Materials, Kyoto, Japan,* July 8-13 2007.
[5] Z. Guo, L. Liu, B. Zhang, S. Du. Critical Void Content for Thermoset Composite Laminates. *Journal of Composite Materials,* 43:1775–1790, 2009.
[6] X. Liu, F. Chen. A review of void formation and its effects on the mechanical performance of carbon fiber reinforced palstic. *Engineering Transactions,* 64:33–51, 2016.
[7] S.F.M. de Almeida, Z.S.N. Neto. Effect of void content on the strength of composite laminates. *Composite Structures,* 28:139–148, 1994.
[8] T.S. Lundström, B.R. Gebart. Influence from process parameters on void formation in resin transfer molding. *Polymer Composites,* 15:25–33, 1994.
[9] T.A. Cender, P. Simacek, S.G. Advani. Resin film impregnation in fabric prepregs with dual length scale permeability. *Composites: Part A,* 53:118–128, 2013.
[10] D. Zhang, D. Heider, J.W. Gillespie Jr.. Role of prepreg interlayer permeability on void reduction during oven vacuum bag processing of thick section thermoplastic composites. *SAMPE Conference Proceedings, Baltimore, MD, USA,* May 18-21 2015.
[11] C. Gouldstone, D. Degtiarov, R.D. Williams. Reinforcing ply drop interfaces using vertically-aligned carbon nanotube forest. *SAMPE Conference Proceedings, Seattle, WA, USA,* June 2-5 2014.
[12] E.J. Garcia, B.L. Wardle, A.J. Hart. Joining prepreg composite interfaces with aligned carbon nanotubes. *Composites: Part A,* 39:1065–1070, 2008.
[13] H. Conway, D. Chebot, C. Gouldstone, R.D. Williams. Fatigue response of carbon fiber epoxy laminates with vertically-alligned carbon nanotube interfacial reinforcement. *SAMPE Conference Proceedings, Baltimore, MD, USA,* May 18-21 2015.
[14] R. Guzmán de Villoria, L. Ydrefors, P. Hallander, K. Ishiguro, P. Nordin, B. L. Wardle. Aligned carbon nanotube reinforcement of aerospace carbon fiber composites: substructural strength evaluation for aerostructure applications. *53rd AIAA/ASME/ASCE/AHS/ASC Structures, Structural Dynamics and Materials Conference, Honolulu, HI, USA,* April 23-26 2012.
[15] H. Zhu, D. Li, D. Zhang, B. Wu, Y. Chen. Influence of voids on interlaminar shear strength of carbon/epoxy fabric laminates. *Transactions of Nonferrous Metals Society of China, 19:s470–s475, 2009.*
[16] J. Kastner, B. Plank, D. Salaberger, J. Sekelja. Defect and porosity determination of fibre reinforced polymers by x-ray Computed Tomography. *2nd Int. Symposium on NDT in Aerospace, Hamburg, Germany,* November 22-24 2010.
[17] J.E. Little, X.W. Yuan, M.I. Jones. Void characterization in carbon fiber/epoxy composite laminates. *Proceedings of the 18th International Conference on Composite Materials, Jeju Island, S. Korea,* August 21-26 2011.
[18] K.J. Bowles, S. Frimpong. Relationship between voids and interlaminar shear strength of polymer matrix composites. *SAMPE Conference Proceedings, San Diego, CA, USA,* April 15-18 1991.
[19] ASTM D 2344 / D2344M-13, Standard Test Method for Short-Beam Strength of Polymer Matrix Composite Materials and Their Laminates. *ASTM International, West Conshohochen, PA, 2013, DOI: 10.1520/D2344_D2344M, www.astm.org.*
[20] ASTM D6484 / D6484M-14, Standard Test Method for Open-Hole Compressive Strength of Polymer Matrix Composite Laminates, *ASTM International, West Conshohocken, PA, 2014, DOI: 10.1520/D6484_D6484M-14, www.astm.org.*

Excerpt from ISBN 978-3-00-053387-7